Heterometallic One-Dimensional Arrays Containing Cyanide-Bridged Lanthanide(III) and Transition Metals

David W. Knoeppel, Jianping Liu, Edward A. Meyers, and Sheldon G. Shore*

Department of Chemistry, The Ohio State University, Columbus, Ohio 43210

Received April 20, 1998

One-dimensional arrays having the general formula $\{(DMF)_{10}Ln_2[M(CN)_4]_3\}_\infty$ [Ln = Sm, Eu, Er, Yb and M = Ni, Pd, Pt] were prepared from the reactions of 2:3 molar ratios of $LnCl_3$ with $K_2[M(CN)_4]$ in DMF (DMF = *N*,*N*-dimethylformamide). Under similar conditions using 1:1 molar ratios of $SmCl_3$ and $K_2[Ni(CN)_4]$ in DMF or $YbCl_3$ and $K_2[Ni(CN)_4]$ in DMA (DMA = *N*,*N*-dimethylacetamide), the one-dimensional arrays $\{(DMF)_5Sm[Ni(CN)_4]Cl\}_\infty$, **8**, and $\{(DMA)_4Yb[Ni(CN)_4]Cl\}_\infty$, **9**, were prepared. An earlier study of $\{(DMF)_{10}Yb[Ni(CN)_4]_3\}_\infty$, **3**, and $\{(DMF)_{10}Yb_2[Pt(CN)_4]_3\}_\infty$, **7**, showed that two different yet related one-dimensional arrays can be adopted. In the present study, X-ray crystal structures of $\{(DMF)_{10}Sm_2[Ni(CN)_4]_3\}_\infty$, **1**, and $\{(DMF)_{10}Er_2[Ni(CN)_4]_3\}_\infty$, **2**, are shown to be isomorphous with $\{(DMF)_{10}Yb_2[Ni(CN)_4]_3\}_\infty$, **3**, while $\{(DMF)_{10}Sm_2[Pd(CN)_4]_3\}_\infty$, **4**, $\{(DMF)_{10}Eu_2[Pd(CN)_4]_3\}_\infty$, **5**, and $\{(DMF)_{10}Yb_2[Pd(CN)_4]_3\}_\infty$, **6**, are isomorphous with $\{(DMF)_{10}Yb_2[Pt(CN)_4]_3\}_\infty$, **7**. Single-crystal X-ray crystal structure determinations reveal that arrays **1**, **2**, and **3** consist of cyanide-bridged "diamond"-shaped Ln_2Ni_2 metal cores. These metal cores are linked together in an infinite array through cyanide bridges by $[Ni(CN)_4]^{2-}$ anions generating a single-strand chain. Crystal data for **1**: triclinic space group $P\bar{1}$, $a = 10.442(5)$ Å, $b = 10.923(2)$ Å, $c = 15.168(3)$ Å, $\alpha = 74.02(2)°$, $\beta = 83.81(3)°$, $\gamma = 82.91(2)°$, $Z = 2$. Crystal data for **2**: triclinic space group $P\bar{1}$, $a = 10.172(1)$ Å, $b = 11.111(3)$ Å, $c = 15.369(2)$ Å, $\alpha = 73.17(2)°$, $\beta = 85.15(1)°$, $\gamma = 83.48(2)°$, $Z = 2$. Arrays **4**, **5**, **6**, and **7** consist of two parallel zigzag chains that are linked together through bridging $[M(CN)_4]^{2-}$ anions. Crystal data for **4**: triclinic space group $P\bar{1}$, $a = 9.304(2)$ Å, $b = 11.351(3)$ Å, $c = 16.257(5)$ Å, $\alpha = 81.62(2)°$, $\beta = 77.51(2)°$, $\gamma = 82.47(2)°$, $Z = 2$. Crystal data for **5**: triclinic space group $P\bar{1}$, $a = 9.300(3)$ Å, $b = 11.353(4)$ Å, $c = 16.279(3)$ Å, $\alpha = 81.58(2)°$, $\beta = 77.37(2)°$, $\gamma = 81.58(2)°$, $Z = 2$. Crystal data for **6**: triclinic space group $P\bar{1}$, $a = 9.164(2)$ Å, $b = 11.718(3)$ Å, $c = 16.122(3)$ Å, $\alpha = 79.88(2)°$, $\beta = 74.43(2)°$, $\gamma = 80.50(2)°$, $Z = 2$. Electrical conductance, NMR, and infrared studies of DMF solutions of **1**−**7** reveal that these arrays are partially ionized in solution. Single-crystal X-ray analyses of the one-dimensional arrays **8** and **9** show that these complexes adopt the commonly observed zigzag chain structure. Crystal data for **8**: monoclinic space group $P2_1/n$, $a = 7.783(2)$ Å, $b = 17.748(8)$ Å, $c = 21.236(5)$ Å, $\beta = 92.87(2)°$, $Z = 4$. Crystal data for **9**: monoclinic space group $P2_1/n$, $a = 10.022(2)$ Å, $b = 19.505(4)$ Å, $c = 15.742(3)$ Å, $\beta = 105.94(2)°$, $Z = 4$. Studies of **8** and **9** in DMF and DMA, respectively, indicate that **8** is partially ionized and **9** is almost completely ionized.

Introduction

Heterometallic complexes are a recurring theme in inorganic and organometallic chemistry as they find uses in both materials applications and in catalysis.[1] Incorporation of two or more different metal atoms into the same complex can be accomplished through the formation of metal−metal bonds, bridging ligands, or as solvent-separated ion pairs. In our studies, we have become increasingly interested in producing heterometallic complexes that contain both lanthanide and transition metals for uses in catalysis or as precursors to heterogeneous catalysts.[2] Direct lanthanide−transition metal bonds are ideal for such purposes. However, bonds between transition metals and electropositive elements such as lanthanides are relatively rare. To date only three X-ray crystal structures have confirmed the presence of direct lanthanide−transition metal bonds.[2b,c,3,4] We have now turned our attention to synthesizing ion-paired complexes using bridging ligands. In a report and preliminary communication, we described investigations using the CN^- anion as a bridging ligand between divalent lanthanide[2e] or trivalent lanthanide cations[2d] and the transition metals nickel or platinum. Here, we provide additional examples of trivalent lanthanide cations with the transition metal anions $[Ni(CN)_4]^{2-}$, $[Pd(CN)_4]^{2-}$, and $[Pt(CN)_4]^{2-}$.

Tetracyanometalate(II) dianions of the nickel triad exist in a range of solid-state structures. When all four cyano groups are

(1) (a) Braunstein, P.; Rose, J. *Stereochem. Organomet. Inorg. Compd.* **1988**, *3*, 320. (b) Boyd, E. P.; Ketchum, D. R.; Deng, H.; Shore, S. G. *Chem. Mater.* **1997**, *9*, 1154.

(2) (a) White, J. P., III; Deng, H.; Boyd, E. P.; Gallucci, J.; Shore, S. G. *Inorg. Chem.* **1994**, *33*, 1685. (b) Deng, H.; Shore, S. G. *J. Am. Chem. Soc.* **1991**, *113*, 8538. (c) Deng, H.; Chun, S.; Florian, P.; Grandinetti, P. J.; Shore, S. G. *Inorg. Chem.* **1996**, *35*, 3891. (d) Knoeppel, D. W.; Shore, S. G. *Inorg. Chem.* **1996**, *35*, 1747. (e) Knoeppel, D. W.; Shore, S. G. *Inorg. Chem.* **1996**, *35*, 5328. (f) White, J. P., III. Ph.D. dissertation, The Ohio State University, Columbus, Ohio, 1990. (g) Deng, H. Ph.D. dissertation, The Ohio State University, Columbus, Ohio, 1991. (h) Knoeppel, D. W. Ph.D. dissertation, The Ohio State University, Columbus, Ohio, 1995. (i) Liu, J. Ph.D. dissertation, The Ohio State University, Columbus, Ohio, 1997.

(3) Magomedov, G. K.; Voskoboynikov, A. Z.; Chuklanova, E. B.; Gusev, A. I.; Beletskaya, I. P. *Metalloorg. Khim.* **1990**, *3*, 706.

(4) Beletskaya, I. P.; Voskoboynikov, A. Z.; Chuklanova, E. B.; Kirillova, N. I.; Shestakova, A. K.; Parshina, I. N.; Gusev, A. I.; Magomedov, G. K.-I. *J. Am. Chem. Soc.* **1993**, *115*, 3156.

S0020-1669(98)00449-2 CCC: $15.00
Published on Web 08/06/1998

bound as monodentate ligands, solvent-separated ion pairs result.[5,6] The bidentate character of two of the four cyano groups of $[M(CN)_4]^{2-}$ has been shown to yield several types of structures in the solid state: molecular,[7] one-dimensional,[2d,e,8] or two-dimensional.[9] When all four cyano ligands are bidentate, a three-dimensional structure can result.[10] We recently reported the first example in which three of the four cyano groups bridge two metal atoms.[2e] Interestingly, no structure has been reported in which one of the four cyano groups acts as a bidentate ligand.

Of the many tetracyanometalate(II) (Ni, Pd, Pt) complexes known, only two tetracyanopalladate(II) structures have been reported that employ lanthanide cations.[11,12] However, no synthetic information nor structural details were given. A series of rare-earth complexes having the general formula $Ln_2[Pt(CN)_4]_3 \cdot xH_2O$ ($x = 18$ or 21) have been reported.[6] Spectroscopic evidence and preliminary X-ray data suggest that these complexes adopt quasi one-dimensional structures that are common to the tetracyanoplatinates(II). We describe here the reactions of $LnCl_3$ with $K_2[M(CN)_4]$ in DMF or DMA. Details of the syntheses and characterization of the one-dimensional arrays $\{(DMF)_{10}Sm_2[Ni(CN)_4]_3\}_\infty$, **1**, $\{(DMF)_{10}Er_2[Ni(CN)_4]_3\}_\infty$, **2**, $\{(DMF)_{10}Yb_2[Ni(CN)_4]_3\}_\infty$, **3**, $\{(DMF)_{10}Sm_2[Pd(CN)_4]_3\}_\infty$, **4**, $\{(DMF)_{10}Eu_2[Pd(CN)_4]_3\}_\infty$, **5**, $\{(DMF)_{10}Yb_2[Pd(CN)_4]_3\}_\infty$, **6**, $\{(DMF)_{10}Yb_2[Pt(CN)_4]_3\}_\infty$, **7**, $\{(DMF)_5Sm[Ni(CN)_4]Cl\}_\infty$, **8**, and $\{(DMA)_4Yb[Ni(CN)_4]Cl\}_\infty$, **9**, are presented.

Results and Discussion

Syntheses of $\{(DMF)_{10}Ln_2[M(CN)_4]_3\}_\infty$, $\{(DMF)_5Sm[Ni(CN)_4]Cl\}_\infty$, and $\{(DMA)_4Yb[Ni(CN)_4]Cl\}_\infty$. Quantitative syntheses of one-dimensional arrays having the general formula $\{(DMF)_{10}Ln_2[M(CN)_4]_3\}_\infty$ were obtained via metathesis reactions of 2:3 molar ratios of $LnCl_3$ with $K_2[M(CN)_4]$ in DMF at room temperature (eq 1). To ensure complete removal of

$$2LnCl_3 + 3K_2[M(CN)_4] \xrightarrow{DMF} \{(DMF)_{10}Ln_2[M(CN)_4]_3\}_\infty + 6KCl \quad (1)$$

M = Ni; Ln = Sm (**1**), Er (**2**), Yb (**3**)
M = Pd; Ln = Sm (**4**), Eu (**5**), Yb (**6**)
M = Pt; Ln = Yb (**7**)

chloride as KCl, long reaction times were employed (5−7 days for **1**, **3**, **4**, **5**, and **7**; up to 2 weeks for **6** and 3 weeks for **2**). The required long metathesis reaction times were in part due to the stability of the inner-sphere coordination complexes $[(DMF)_7LnCl]^{2+}$ and $[(DMF)_6LnCl_2]^+$.[13] The low solubility of $ErCl_3$ and $YbCl_3$ in DMF also contributed to the long reaction times in the syntheses of **2**, **3**, **6**, and **7**.

In a manner similar to the syntheses described for arrays **1**−**7**, the one-dimensional arrays **8** and **9** were obtained via the metathesis reactions of equal molar amounts of $SmCl_3$ and $K_2[Ni(CN)_4]$ in DMF (eq 2) or $YbCl_3$ and $K_2[Ni(CN)_4]$ in DMA (eq 3). Once the metathesis reactions were complete (eqs 1−3),

$$SmCl_3 + K_2[Ni(CN)_4] \xrightarrow{DMF} \underset{\mathbf{8}}{\{(DMF)_5Sm[Ni(CN)_4]Cl\}_\infty} + 2KCl \quad (2)$$

$$YbCl_3 + K_2[Ni(CN)_4] \xrightarrow{DMA} \underset{\mathbf{9}}{\{(DMA)_4Yb[Ni(CN)_4]Cl\}_\infty} + 2KCl \quad (3)$$

each of the one-dimensional arrays (**1**−**9**) was isolated as discrete single crystals from concentrated DMF solutions.

Molecular Structures of the One-Dimensional Arrays $\{(DMF)_{10}Ln_2[M(CN)_4]_3\}_\infty$. From single-crystal X-ray analyses, the molecular structures of the complexes were shown to possess the general formula $\{(DMF)_{10}Ln_2[M(CN)_4]_3\}_\infty$ with two different, yet related, one-dimensional structures, which we designate as type **A** and type **B**. Complexes that adopt the structural type **A** are **1**, **2**, and **3**. Complexes that adopt the structural type **B** are **4**, **5**, **6**, and **7**. Since the structures of the members of the type **A** complexes are isomorphous, only the molecular structure of **2** is discussed in detail here. The structure of complex **3** has already been described elsewhere[2d] and the details of structure **1** are provided in the Supporting Information. By the same token, of the type **B** complexes only the structure of **6** is discussed in detail here. For the other type **B** complexes, isomorphous couterparts of **6**, the structure of complex **7** has been described elsewhere[2d] and structural details for **4** and **5** are provided in the Supporting Information that is associated with this article.

The molecular structures of **2** (type **A**) and **6** (type **B**) are shown in Figures 1 and 2, respectively. The unit cell packing for **6** is displayed in Figure 3. Crystallographic data for **2** and **6** are listed in Table 1. Selected bond distances and angles for **2** and **6** are given in Table 2. Complexes **A** and **B** not only have the same general formula, they also have the same asymmetric unit $\{[M(CN)_2]Ln(DMF)_5[M(CN)_4]\}$ (**I**), which is operated on at an inversion center on M to give the same repeating unit $\{[M(CN)_4](DMF)_5Ln[M(CN)_4]Ln(DMF)_5[M(CN)_4]\}$ (**II**) in the array. The difference between these two structures arises from the way in which the repeating units combine to form arrays as shown in Scheme 1.

In the type **A** structure, the one-dimensional array is generated by translating the repeating unit along the *ac* diagonals of the lattice. Here, two $[Ni(CN)]^{2-}$ anions bridge two Er(III) ions in a cis fashion, creating "diamond"-shaped Er_2Ni_2 metal cores that are held together by cyanide bridges. These "diamond"-shaped cores are then linked by $[Ni(CN)_4]^{2-}$ anions which are bound to the erbium atoms through cyanide bridges in a trans fashion (Figure 1). Unlike **A**, the repeating unit of **B** is translated only along the crystallographic *a* axis of the lattice. The structure consists of two inverted parallel zigzag chains that are linked by $[Pd(CN)_4]^{2-}$ anions. These zigzagging chains are generated by $[Pd(CN)_4]^{2-}$ ions that bridge the Yb(III) ions in a cis fashion. The chains are then connected through the ytterbium atoms by trans bridging $[Pd(CN)_4]^{2-}$ anions (Figure 2).

At this time it is unclear what conditions dictate which structural type **A** or **B** is adopted. However, it is apparent that the coordination around the lanthanide atom governs the structural type adopted for each array. In each of the five structures (**1**, **2**, **4**, **5**, and **6**) reported here and in the previously

(5) Cernak, J.; Chomic, J.; Dunaj-Jurco, M.; Kappenstein, C. *Inorg. Chim. Acta* **1984**, *85*, 219.
(6) Glieman, G.; Yersin, H. *Struct. Bond.* **1985**, *62*, 87 and references therein.
(7) Cernak, J.; Chomic, J.; Dunaj-Jurco, M. *Chem. Papers* **1990**, *44*, 13.
(8) Cernak, J.; Potocnak, I.; Chomic, J.; Dunaj-Jurco, M. *Acta Crystallogr.* **1990**, *C46*, 1098.
(9) Yuge, H.; Iwamoto, T. *Acta Crystallogr.* **1995**, *C51*, 374.
(10) Gable, R. W.; Hoskins, B. F.; Robson, R. *J. Chem. Soc., Chem. Commun.* **1990**, 762.
(11) Klement, U. Z. *Kristallogr.* **1993**, *208*, 285.
(12) Klement, U. Z. *Kristallogr.* **1993**, *208*, 288.
(13) Ishiguro, S.; Takahashi, R. *Inorg. Chem.* **1991**, *30*, 1854.

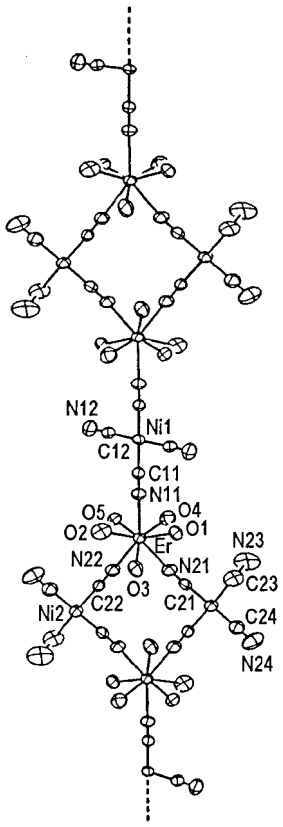

Figure 1. Molecular structure (50% thermal ellipsoids) of a portion of the one-dimensional array **2** (only the oxygen atoms of the DMF shown for clarity).

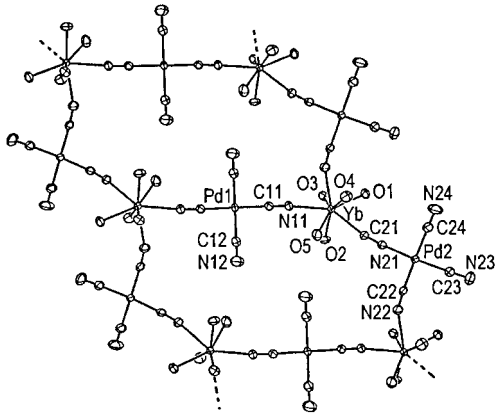

Figure 2. Molecular structure (50% thermal ellipsoids) of a portion of the one-dimensional array **6** (only the oxygen atoms of the DMF shown for clarity).

reported structures **3** and **7**,[2d] the lanthanide ions are bound to three N atoms of the bridging cyanide ions and five O atoms of the DMF ligands. The coordination geometry around each of the lanthanide atoms is a slightly distorted square antiprism (Figure 4). Two of the coordinated N atoms share an edge of one of the bases of the antiprism, while the third N atom occupies a corner of the other base opposite the shared edge. In array **2** (type **A**) the edge sharing N atoms (N21 and N22) of the square antiprism are donated by two cyanide ligands of two cis bridging $[M(CN)_4]$ units, while the third N atom (N11) is from a cyanide ligand of a trans bridging $[M(CN)_4]$ unit (Figure 4a). In array **6** (type **B**), one of the edge sharing N atoms (N22) comes from a cyanide ligand of a cis bridging $[M(CN)_4]$ unit and the other (N11) is from a cyanide ligand of a trans bridging $[M(CN)_4]$ unit. The third N atom (N21) is thus donated by a cyanide ligand of a cis bridging $[M(CN)_4]$ unit (Figure 4b).

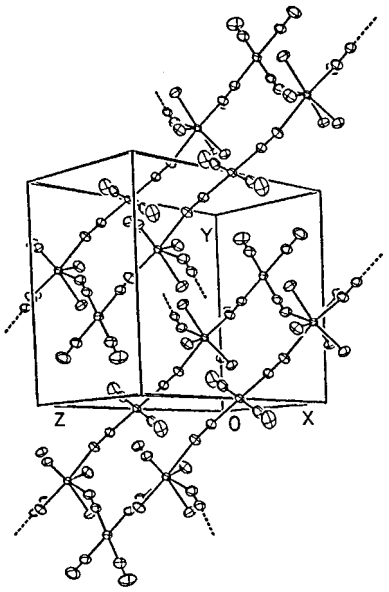

Figure 3. Unit cell packing diagram of **6** with 50% thermal ellipsoids (only the oxygen atoms of the DMF shown for clarity).

Table 1. Crystallographic Data for **2** and **6**

empirical formula	$C_{42}H_{70}O_{10}N_{22}Er_2Ni_3$, **2** (type **A**)	$C_{42}H_{70}N_{22}O_{10}Yb_2Pd_3$, **6** (type **B**)
fw	1553.82	1708.48
space group	$P\bar{1}$	$P\bar{1}$
a, Å	10.172(1)	9.164(2)
b, Å	11.111(3)	11.718(3)
c, Å	15.369(2)	16.122(3)
α, deg	73.17(2)	79.88(2)
β, deg	85.15(1)	74.43(2)
γ, deg	83.48(2)	80.50(2)
V, Å^3	1649.4(6)	1634.8(2)
Z[a]	2	2
ρ (calcd), g·cm^{-3}	1.623	1.736
crystal size, mm	0.10 × 0.20 × 0.25	0.32 × 0.21 × 0.20
λ, Å	Mo Kα (0.710 73)	Mo Kα (0.710 73)
T, °C	room temp	−60
μ, cm^{-1}	34.5	37.06
transm coeff.	0.6551−0.9994	0.4414−0.5990
R_1	0.026[b]	0.0197[d]
R_2	0.030[c]	0.0481[e]

[a] The asymmetric unit for these complexes consists of $C_{21}H_{35}O_5N_{11}LnM_{1.5}$ (Ln = Er, Yb; M = Ni, Pd), and there are two asymmetric units per unit cell. [b] $R_F = \sum||F_o| - |F_c||/\sum|F_o|$. [c] $R_{wF} = \{\sum w[|F_o| - |F_c|]^2/\sum w|F_o|^2\}^{1/2}$. [d] $R_1 = \sum||F_o| - |F_c||/\sum|F_o|$. [e] $wR_2 = \{\sum[w(F_o^2 - F_c^2)^2]/\sum[w(F_o^2)^2]\}^{1/2}$.

The average Ln−N bond distances are 2.44[1][14] and 2.44[2][14] Å for **2** and **6**, while the average Ln−O bond distances are 2.32[1][14] and 2.30[1][14] Å for **2** and **6**. The average bond distances of Er−N (2.44[1][14] Å) and Er−O (2.32[1][14] Å) in **2** compares with the average distances of Er−N (2.42[2][14] Å) and Er−O (2.319(4) Å) reported for the eight-coordinate Er(III) ion in $ErFe(CN)_6 \cdot 4H_2O$.[15] The average Yb−N and Yb−O bond distances in **6** are comparable to those observed in complexes **3** and **7**.[2d]

(14) Stout, G. H.; Jensen, L. H. In *X-ray Structure Determination*; 2nd ed.; Wiley: New York, 1989; pp 406−408. The standard deviation (σ_l) for the average Ln−N and Ln−O bond lengths calculated according to the following equations from this reference: $\langle l \rangle = \sum_m l_m/m$; $\sigma_l = [\sum_m (l_m - \langle l \rangle)^2/m(m-1)]^{1/2}$, where $\langle l \rangle$ is the mean length, l_m is the length of the mth bond, and m is the number of bonds.

Table 2. Selected Bond Distances (Å) and Angles (deg) and Their Esd's for **2** and **6**

$\{(DMF)_{10}Er_2[Ni(CN)_4]_3\}_\infty$, **2**[a] (type **A**)		$\{(DMF)_{10}Yb_2[Pd(CN)_4]_3\}_\infty$, **6**[b] (type **B**)	
Bond Distances			
Er−O1	2.293(4)	Yb−O1	2.303(2)
Er−O2	2.318(4)	Yb−O2	2.310(2)
Er−O3	2.310(5)	Yb−O3	2.341(2)
Er−O4	2.359(5)	Yb−O4	2.279(3)
Er−O5	2.295(5)	Yb−O5	2.272(2)
Er−N11	2.458(5)	Yb−N11	2.406(3)
Er−N21	2.448(5)	Yb−N21	2.461(3)
Er−N22	2.424(5)	Yb−N22#1	2.464(3)
Ni1−C11	1.854(6)	Pd1−C11	1.989(3)
Ni1−C12	1.862(7)	Pd1−C12	1.986(4)
Ni2−C21	1.847(6)	Pd2−C21	1.992(4)
Ni2−C22	1.859(6)	Pd2−C22	2.000(4)
Ni2−C23	1.869(8)	Pd2−C23	2.001(4)
Ni2−C24	1.857(7)	Pd2−C24	1.991(4)
N11−C11	1.156(7)	C11−N11	1.142(4)
N12−C12	1.134(8)	C12−N12	1.136(5)
N21−C21	1.136(7)	C21−N21	1.143(4)
N22−C22	1.161(7)	C22−N22	1.142(5)
N23−C23	1.151(9)	C23−N23	1.140(5)
N24−C24	1.154(8)	C24−N24	1.138(5)
Bond Angles			
O1−Er−O2	110.5(2)	O1−Yb−O2	103.35(9)
O1−Er−O3	73.9(2)	O1−Yb−O3	73.29(9)
O1−Er−O4	80.7(2)	O1−Yb−O4	83.1(1)
O1−Er−O5	144.6(2)	O1−Yb−O5	141.26(9)
O1−Er−N11	73.9(2)	O1−Yb−N21	70.19(9)
O1−Er−N21	141.9(2)	O1−Yb−N11	144.82(9)
O1−Er−N22	76.2(2)	O1−Yb−N22#1	76.6(1)
O2−Er−O3	70.3(2)	O2−Yb−O3	71.92(8)
O2−Er−O4	141.7(2)	O2−Yb−O4	145.03(9)
O2−Er−O5	78.8(2)	O2−Yb−O5	80.9(1)
O2−Er−N11	71.8(2)	O2−Yb−N11	84.8(1)
O2−Er−N21	81.0(2)	O2−Yb−N21	74.81(9)
O2−Er−N22	143.3(2)	O2−Yb−N22#1	143.5(1)
O3−Er−O4	145.8(2)	O3−Yb−O4	141.14(9)
O3−Er−O5	138.7(2)	O3−Yb−O5	141.35(9)
O3−Er−N11	116.1(2)	O3−Yb−N21	122.2(1)
O3−Er−N21	76.7(2)	O3−Yb−N11	77.09(9)
O3−Er−N22	77.7(2)	O3−Yb−N22#1	73.3(1)
O4−Er−O5	73.1(2)	O4−Yb−O5	73.7(1)
O4−Er−N11	77.0(2)	O4−Yb−N21	75.4(1)
O4−Er−N21	113.3(2)	O4−Yb−N11	109.8(1)
O4−Er−N22	74.2(2)	O4−Yb−N22#1	71.4(1)
O5−Er−N11	77.2(2)	O5−Yb−N21	74.1(1)
O5−Er−N21	72.1(2)	O5−Yb−N11	73.4(1)
O5−Er−N22	117.5(2)	O5−Yb−N22#1	122.3(1)
N11−Er−N21	142.2(2)	N11−Yb−N21	143.9(1)
N11−Er−N22	141.2(2)	N21−Yb−N22#1	135.1(1)
N21−Er−N22	74.3(2)	N11−Yb−N22#1	77.1(1)
Er−N11−C11	177.6(5)	Yb−N11−C11	165.7(3)
Er−N21−C21	170.3(5)	Yb#3−N22−C22	156.7(3)
Er−N22−C22	174.5(5)	Yb−N21−C21	169.6(3)
C11−Ni1−C11	180	C11#2−Pd1−C11	180
C11−Ni1−C12	89.1(2)	C11−Pd1−C12	89.7(1)
C12−Ni1−C12	180	C12−Pd1−C12#2	180
C21−Ni2−C22	91.4(2)	C21−Pd2−C22	92.8(1)
C21−Ni2−C23	172.4(4)	C21−Pd2−C23	176.4(1)
C21−Ni2−C24	89.1(3)	C21−Pd2−C24	88.4(1)
C22−Ni2−C23	89.1(3)	C22−Pd2−C23	89.8(1)
C22−Ni2−C24	176.9(3)	C22−Pd2−C24	177.8(2)
C23−Ni2−C24	90.7(3)	C23−Pd2−C24	89.1(2)
Ni1−C11−N11	178.2(5)	Pd1−C11−N11	176.2(3)
Ni1−C12−N12	177.8(6)	Pd1−C12−N12	178.7(4)
Ni2−C21−N21	174.7(6)	Pd2−C21−N21	174.6(3)
Ni2−C22−N22	177.3(5)	Pd2−C22−N22	174.6(3)
Ni2−C23−N23	175(1)	Pd2−C23−N23	177.8(4)
Ni2−C24−N24	178.8(8)	Pd2−N24−C24	178.3(4)

[a] Bond distances and angles were calculated for symmetry-related atoms by applying the inversion operation on complex **2**. [b] Symmetry transformations used to generate equivalent atoms: #1, $x-1, y, z$; #2, $-x, -y, -z+1$; #3, $x+1, y, z$.

The coordination geometries around the nickel and palladium atoms in **2** and **6** are all approximately square planar. The widest C−M−C bond angles in structural types **A** (91.4(2)° for complex **2**) and **B** (92.8(1)° for complex **6**) are the C21-M−C22 angles (M = Ni, Pd) that bridge in a cis fashion to two sterically crowded lanthanide atoms. To bridge these two lanthanide atoms, the C21−M−C22 angle is opened, though this does not affect the linearity of the M−C≡N bonds ranging from 175(1) to 178.8(8)° for **2** and from 174.6(3) to 178.7(4)° for **6**. In contrast, the Ln−N≡C bond angles vary with regard to linearity ranging from 170.3(5) to 177.6(5)° for **2** and from 156.7(3) to 169.6(3)° for **6**. This is most likely due to steric crowding around the Ln(III) cations. The M−C and C≡N bond lengths also vary with regard to bridging and terminal modes, but are considered normal[6,16] with no statistically significant variations.

Structures of the One-Dimensional Arrays 8 and 9. Crystal data for **8** and **9** are given in Table 3. Selected bond distances and angles for **8** and **9** are reported in Table 4. Unlike **1**−**7**, the structures of **8** and **9** consist of one-dimensional arrays that crystallize in the monoclinic space group $P2_1/n$. The asymmetric unit of **8** is $\{(DMF)_5Sm[Ni(CN)_2]_2Cl\}$. The two Ni atoms in this unit lie on inversion centers. Applying this symmetry operation gives the repeating unit $\{(DMF)_5Sm[Ni(CN)_4]_2Cl\}$ of the array which translates along the crystallographic *c* axis of the lattice to generate a zigzag single-strand chain (Figure 5a). The asymmetric unit of **9**, $\{(DMA)_4Yb[Ni(CN)_4]Cl\}$, is also the repeating unit. It lies along an *n*-glide plane. By applying this symmetry operation to the asymmetric unit, a zigzag single-strand chain is also generated (Figure 5b).

Like the lanthanides in structures **1**−**7**, the Sm(III) ion in **8** is eight-coordinate having a slightly distorted square antiprismatic coordination geometry (Figure 6a). The Sm(III) ion is bound to two N atoms of the bridging cyanides and five O atoms of the DMF ligands. In addition, it is bound to one chloride ion. One N atom is located on each base, and each of the N atoms share one edge of the antiprism with the chloride ion. The O atoms occupy the remaining five vertexes. The Sm−N and Sm−O bond lengths are comparable to those in arrays **A** and **B**. The Sm−Cl bond distance of 2.729(2) Å is similar to the average bond distance for the two crystallographically independent molecules in $(C_5(CH_3)_5)_2SmCl(THF)$ (2.737 Å).[17]

Unlike **8**, the ytterbium atom in **9** is seven-coordinate, with a pentagonal bipyramidal arrangement (Figure 6b). This is probably due to the smaller ionic radius of Yb(III) compared to that of Sm(III) and also the increase in steric requirements for the DMA ligand versus the DMF ligand. The Yb(III) ion in **9** is bound to two N atoms of the bridging cyanide ions and three O atoms of the DMA ligands at the equatorial vertexes. The remaining DMA ligand and the chloride ion occupy the apexes trans to each other. The average Yb−O bond distance of 2.23[3] Å in **9** is shorter than the average Yb−O bond distances in arrays **3** and **7** by 0.06 and 0.07 Å.[2d] This is in good agreement with the expected differences in ionic radii between seven and eight coordinate Yb(III).[18] Surprisingly, the average Yb−N bond distance of 2.414[7] Å is not much less than those in arrays **3** and **7**.[2d] This may in part may be due to the increase in steric requirements of the competitively coor-

(15) Dommann, A.; Vetsch, H.; Hulliger, F. Petter, W. *Acta Crystallogr.* **1990**, *C46*, 1992.
(16) Cernak, J.; Dunaj-Jurco, M.; Melnik, M.; Chomic, J.; Skorsepa, J. *Rev. Inorg. Chem.* **1988**, *9*, 259.
(17) Evans, W. J.; Grate, J. W.; Levan, K. R.; Bloom, I.; Peterson, T. T.; Doedens, R. J.; Zhang, H.; Atwood, J. L. *Inorg. Chem.* **1986**, *25*, 3614.
(18) Shannon, R. D. *Acta Crystallogr.* **1976**, *A32*, 751.

Scheme 1

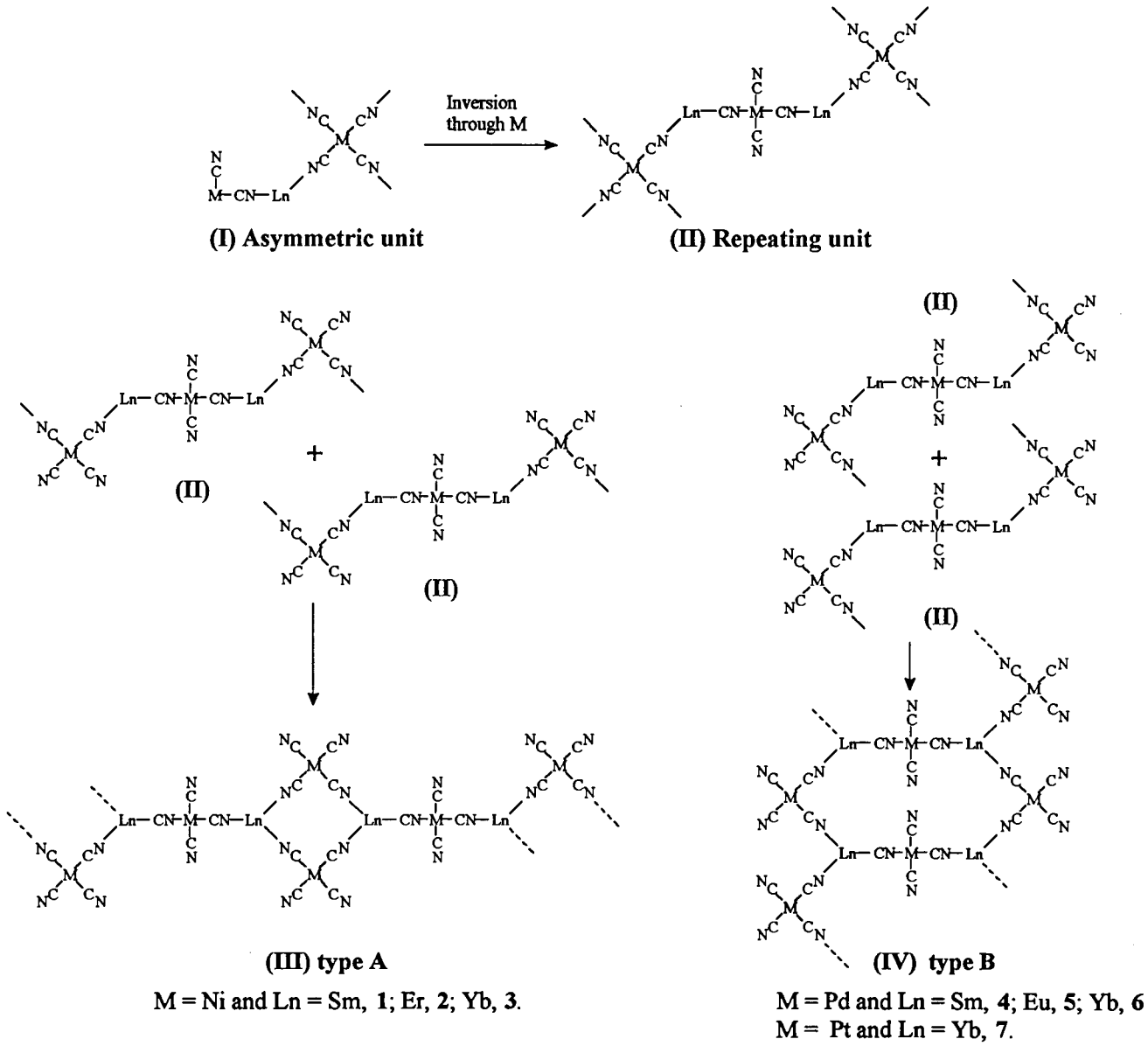

dinating DMA ligands. As expected, the average Yb−Cl bond lengths in the six-coordinate complexes $YbCl_3(C_6H_{10}O_2)(THF)_2$ (2.527 Å) ($C_6H_{10}O_2$ = ϵ-caprolactone)[19] and $YbCl_3(THF)_3$ (2.52 Å)[20] are slightly shorter than the Yb−Cl bond distance of 2.576(2) Å in **9**. The differences are in good agreement with the difference reported for six and seven coordinate Yb(III).[17]

The coordination geometries around the transition metal atoms in **8** and **9** are all approximately square planar. The C−Ni−C angles range from 88.5(3) to 91.5(3)° for **8** and from 88.1(4) to 92.2(4)° for **9**. The Ni−C≡N and Ln−N≡C bond angles for **8** and **9** are nearly linear except for the Yb−N13≡C13 bond angle in **9** which deviates slightly from linearity [162.5(7)°]. This is most likely due to steric crowding around the ytterbium atom. The Ni−C and C≡N bond lengths in **8** and **9** are normal.[16]

Spectroscopic Studies of Complexes of Type A, 1−3, and Type B, 4−7. The Experimental Section lists the observed infrared absorption frequencies for both Nujol mull and DMF solutions of **1**−**7** in the CN stretching region.

Solid-state infrared spectra appear to be useful in distinguishing between the type **A** and type **B** structures. Figure 7 shows infrared spectra of these two structural types.

The infrared spectra for type **A** complexes in Nujol mull contain bands that are higher than the normal modes for the cyanide ligand in $K_2[Ni(CN)_4]$ (2127 cm^{-1}).[21] They are assigned to bridging cyanide stretching frequencies. Typically bridging CN ligands have higher stretching frequencies than the terminal CN ligands.[22] The remaining CN stretches are attributed to the nonbridging cyanide ligands because their location in the cyanide stretching region compares with the absorptions observed for the non bridging cyanide ligands in $K_2[Ni(CN)_4]$. Similarly, in the type **B** complexes cyanide stretching bands at higher frequencies than the stretching modes of $K_2[Pd(CN)_4]\cdot H_2O$ (2134 cm^{-1})[21] and $K_2[Pt(CN)_4]\cdot 3H_2O$

(19) Evans, W. J.; Shreeve, J. L.; Ziller, J. W.; Doedens, R. J. *Inorg. Chem.* **1995**, *34*, 576.
(20) Deacon, G. B.; Feng, T.; Nickel, S.; Skelton, B. W.; White, A. H. *J Chem. Soc., Chem. Commun.* **1993**, 1328.
(21) Kubas, G. J.; Jones, L. H. *Inorg. Chem.* **1974**, *13*, 2186.
(22) Nakamoto, K. *Infrared and Raman Spectra of Inorganic and Coordination Compounds, Part B*, 5th ed.; Wiley and Sons: New York, 1997; pp 105−113 and references therein.

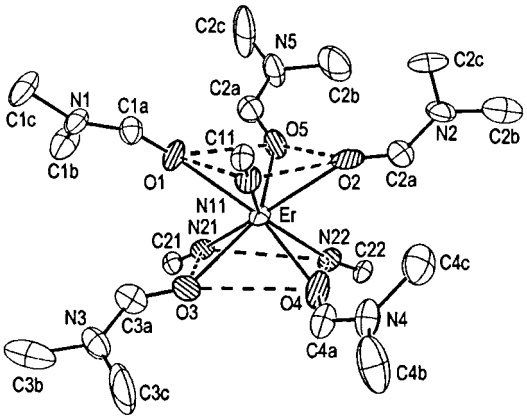

(a) $\{(DMF)_{10}Er_2[Ni(CN)_4]_3\}_\infty$, **2**

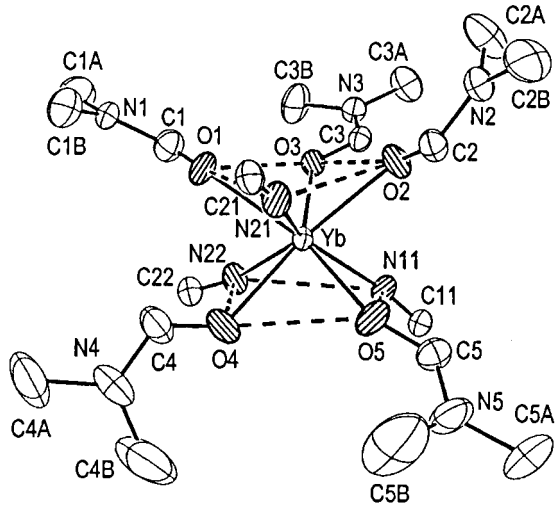

(b) $\{(DMF)_{10}Yb_2[Pd(CN)_4]_3\}_\infty$, **6**

Figure 4. Coordination geometry around the lanthanide atoms in (a) **2** and (b) **6**.

Table 3. Crystallographic Data for **8** and **9**

empirical formula	$C_{19}H_{35}SmNiClO_5N_9$, **8**	$C_{20}H_{36}N_8O_4YbNiCl$, **9**
fw	714.06	719.74
space group	$P2_1/n$	$P2_1/n$
a, Å	7.783(2)	10.022(2)
b, Å	17.748(8)	19.505(4)
c, Å	21.236(5)	15.742(3)
β, deg	92.87(2)	105.94(2)
V, Å^3	2930(2)	2959(4)
Z	4	4
ρ (calcd), g cm^{-3}	1.752	1.616
T, °C	−60	−60
λ, Å	0.71073	0.71073
μ, cm^{-1}	27.7	38.2
transm coeff.	0.6612−0.9995	0.6806−0.9995
R_F[a]	0.029	0.027
R_{wF}[b]	0.033	0.031

[a] $R_F = \sum||F_o| - |F_c||/\sum|F_o|$. [b] $R_{wF} = \{\sum w[|F_o| - |F_c|]^2/\sum w|F_o|^2\}^{1/2}$.

(2134 cm^{-1})[21] are assigned to bridging cyanide ligands, while the band that occurs at around 2134 cm^{-1} in the type **B** complexes is assigned to terminal cyanide ligands.

Solution infrared spectra of type **A** and type **B** complexes in DMF differ from their solid state infrared spectra, thereby establishing that the species in the solid state are not those in solution (Figure 8). Upon recrystallization, however, self-assembly occurs and the type **A** and **B** solids are recovered.

Table 4. Selected Bond Distances (Å) and Angles (deg) and Their Esd's for **8** and **9**

$\{(DMF)_5Sm[Ni(CN)_4]Cl\}_\infty$, **8**		$\{(DMA)_4Yb[Ni(CN)_4]Cl\}_\infty$, **9**	
Bond Distances			
Sm−Cl	2.729(2)	Yb−Cl	2.576(2)
Sm−O1	2.451(5)	Yb−O1	2.271(5)
Sm−O2	2.340(5)	Yb−O2	2.197(6)
Sm−O3	2.399(5)	Yb−O3	2.231(5)
Sm−O4	2.479(5)	Yb−O4	2.226(6)
Sm−O5	2.387(5)	Yb−N11	2.409(6)
Sm−N11	2.557(6)	Yb−N13	2.419(6)
Sm−N21	2.542(6)	Ni−C11	1.876(9)
Ni1−C11	1.862(8)	Ni−C12	1.86(1)
Ni1−C12	1.86(1)	Ni−C13	1.880(9)
Ni2−C21	1.860(8)	Ni−C14	1.86(1)
Ni2−C22	1.860(9)	N11−C11	1.157(9)
N11−C11	1.152(9)	N12−C12	1.17(1)
N12−C12	1.16(1)	N13−C13	1.149(9)
N21−C21	1.151(9)	N14−C14	1.16(1)
N22−C22	1.14(1)		
Bond Angles			
Cl−Sm−O1	74.8(1)	Cl−Yb−O1	94.2(2)
Cl−Sm−O2	84.7(2)	Cl−Yb−O2	177.7(2)
Cl−Sm−O3	143.0(1)	Cl−Yb−O3	93.9(2)
Cl−Sm−O4	143.3(1)	Cl−Yb−O4	94.6(2)
Cl−Sm−O5	107.0(1)	Cl−Yb−N11	87.0(2)
Cl−Sm−N11	80.8(2)	Cl−Yb−N13	91.6(2)
Cl−Sm−N21	76.9(2)	O1−Yb−O2	88.1(2)
O1−Sm−O2	142.0(2)	O1−Yb−O3	71.1(2)
O1−Sm−O3	72.1(2)	O1−Yb−O4	142.7(2)
O1−Sm−O4	139.4(2)	O1−Yb−N11	143.0(2)
O1−Sm−O5	70.8(2)	O1−Yb−N13	70.4(2)
O1−Sm−N11	74.0(2)	O2−Yb−O3	86.2(2)
O1−Sm−N21	125.9(2)	O2−Yb−O4	84.0(3)
O2−Sm−O3	112.2(2)	O2−Yb−N11	90.9(2)
O2−Sm−O4	72.2(2)	O2−Yb−N13	89.8(2)
O2−Sm−O5	146.8(2)	O3−Yb−O4	144.0(2)
O2−Sm−N11	71.4(2)	O3−Yb−N11	72.0(2)
O2−Sm−N21	78.0(2)	O3−Yb−N13	141.4(2)
O3−Sm−O4	73.5(2)	O4−Yb−N11	73.6(2)
O3−Sm−O5	77.3(2)	O4−Yb−N13	73.1(2)
O3−Sm−N11	74.6(2)	N11−Yb−N13	146.5(2)
O3−Sm−N21	137.2(2)	C11−Ni−C12	88.2(4)
O4−Sm−O5	81.1(2)	C11−Ni−C13	178.3(4)
O4−Sm−N11	116.3(2)	C11−Ni−C14	92.2(4)
O4−Sm−N21	70.7(2)	C12−Ni−C13	91.4(4)
O5−Sm−N11	140.2(2)	C12−Ni−C14	179.3(4)
O5−Sm−N21	74.8(2)	C13−Ni−C14	88.1(4)
N11−Sm−N21	143.4(2)	Yb−N11−C11	174.6(7)
C11−Ni1−C11	180.(0)	Yb−N13−C13	162.5(7)
C11−Ni1−C12	90.6(3)	Ni−C11−N11	176.7(8)
C11−Ni1−C12	89.4(3)	Ni−C12−N12	178.(1)
C12−Ni1−C12	180.(0)	Ni−C13−N13	177.0(8)
C21−Ni2−C21	180.(0)	Ni−C14−N14	177.5(8)
C21−Ni2−C22	88.5(3)		
C21−Ni2−C22	91.5(3)		
C22−Ni2−C22	180.(0)		
Sm−N11−C11	178.3(6)		
Sm−N21−C21	171.2(6)		
Ni1−C11−N11	177.2(7)		
Ni1−C12−N12	178.4(7)		
Ni2−C21−N21	176.7(7)		
Ni2−C22−N22	177.9(8)		

Solutions of the type **A** and **B** complexes contain CN stretching bands at higher frequencies than those for terminal CN stretches, thereby indicating that some of the ion paired complexes through cyanide bridges are present (Figure 8). If complete ionization were taking place, only one absorption due to CN of $[Ni(CN)_4]^{2-}$, $[Pt(CN)_4]^{2-}$, or $[Pt(CN)_4]^{2-}$ would be present in the infrared spectra.

The ^{13}C NMR spectra of DMF solutions of **1**, **2**, and **3** show only one resonance at 131.6, 121.7, and 129.7, respectively due to $[Ni(CN)_4]^{2-}$. Each of these resonances is shifted upfield from

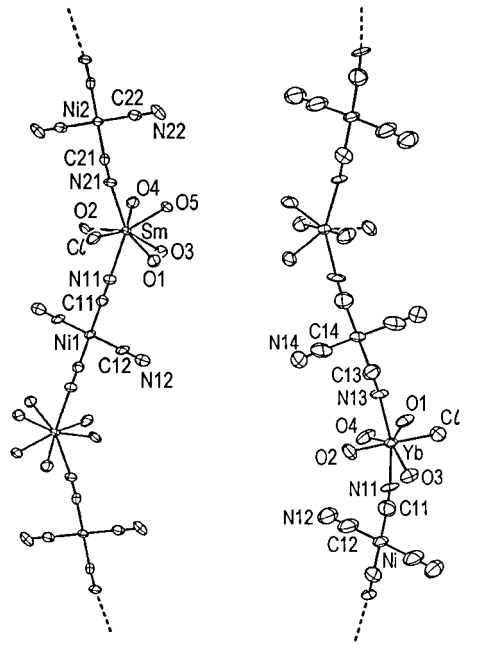

(a) $\{(DMF)_5Sm[Ni(CN)_4]Cl\}_\infty$, **8** (b) $\{(DMA)_4Yb[Ni(CN)_4]Cl\}_\infty$, **9**

Figure 5. Molecular structures (50% thermal ellipsoids) of a portion of the one-dimensional arrays: (a) **8** and (b) **9** (only the oxygen atoms of the DMF and DMA are shown in (a) and (b) for clarity).

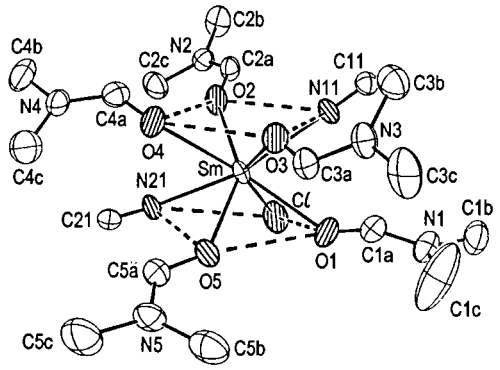

(a) $\{(DMF)_5Sm[Ni(CN)_4]Cl\}_\infty$, **8**

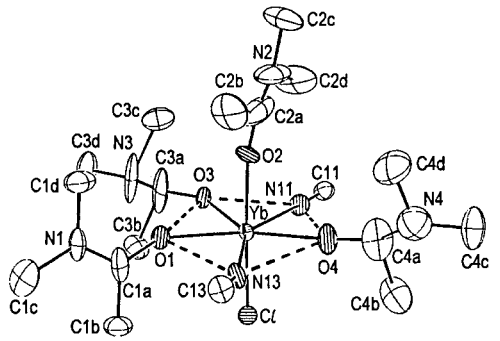

(b) $\{(DMA)_4Yb[Ni(CN)_4]Cl\}_\infty$, **9**

Figure 6. (a) Square antiprism geometry of the Sm(III) ion in **8**. (b) Pentagonal bipyramidal geometry of the Yb(III) ion in **9**.

that of $K_2[Ni(CN)_4]$ in DMF (132.07 ppm).[23] The ^{13}C NMR spectrum of **7** consists of a three line pattern due to $[Pt(CN)_4]^{2-}$. This resonance is centered at 121.20 ppm ($^1J(^{195}PtC) = 1016$ Hz) and is shifted slightly upfield from that of $K_2[Pt(CN)_4]$ in DMF (122.50 ppm ($^1J(^{195}PtC) = 1008$ Hz).[23] The ^{195}Pt NMR spectrum of **7** consists of only one signal at -4702 ppm. This is comparable to the ^{195}Pt NMR spectrum of $K_2[Pt(CN)_4]$ in DMF (-4672 ppm).[23]

Table 5. Molar Conductivities of Complexes in 1 mM DMF Solutions

complex	molecular weight[a]	molar conductivity ($cm^2\ \Omega^{-1}\ mol^{-1}$)[b]
$\{(DMF)_{10}Sm_2[Ni(CN)_4]_3\}_\infty$, **1**	1446.86	114
$\{(DMF)_{10}Er_2[Ni(CN)_4]_3\}_\infty$, **2**	1401.56	107
$\{(DMF)_{10}Yb_2[Ni(CN)_4]_3\}_\infty$, **3**	1486.22	102
$\{(DMF)_{10}Sm_2[Pd(CN)_4]_3\}_\infty$, **4**	1587.05	118
$\{(DMF)_{10}Eu_2[Pd(CN)_4]_3\}_\infty$, **5**	1590.27	117
$\{(DMF)_{10}Yb_2[Pd(CN)_4]_3\}_\infty$, **6**	1632.41	107
$\{(DMF)_{10}Yb_2[Pt(CN)_4]_3\}_\infty$, **7**	1901.39	108

[a] The molecular weight is based on the molecular repeating unit of $\{(DMF)_xLn_2[M(CN)_4]_3\}$ ($x = 8$ for **2** and $x = 9$ for the other complexes). The elemental analysis showed the loss of two DMF ligands per repeating unit for **2** and one DMF ligand per repeating unit for the other complexes after the samples were evacuated for 12 h. [b] Molar conductivities were obtained from plots of Λ vs $C^{1/2}$. The plots were linear.

The existence of a single resonance in the solution ^{13}C NMR spectra of **1**, **2**, **3**, and **7** and the existence of solution infrared data that indicate the presence of bridging cyanides as well as terminal cyanide ligands provide evidence that the making and breaking of lanthanide−cyanide bridge bonds is averaged on the ^{13}C NMR time scale. This evidence correlates with the solution infrared data that indicate that ion paired complexes exist through cyanide bridges. If these complexes consisted of static structures, multiple resonances would be expected in the ^{13}C NMR spectra and possibly in the ^{195}Pt NMR spectrum of **7**.

Since the infrared and ^{13}C NMR studies indicate that complexes **1**−**7** dissociate in DMF solution, it is of interest to measure the molar conductivities of the solutions. Results are summarized in Table 5. These values are intermediate between those expected for a 1:1 electrolyte (65−90 $cm^2\ \Omega^{-1}\ mol^{-1}$) and for a 2:1 electrolyte (130−170 $cm^2\ \Omega^{-1}\ mol^{-1}$) in DMF.[24] These results are consistent with infrared data in solution which indicate that complete dissociation does not occur. From the data in Table 5, the molar conductivities appear to be governed by the sizes of the lanthanide ions. They decrease with decreasing size of the lanthanide ion (Sm(III) ≈ Eu(III) > Er(III) > Yb(III)). These results are consistent with earlier observations.[25]

Spectroscopic Studies of Complexes 8 and 9. The Experimental Section lists the observed infrared absorption frequencies for both Nujol mull and DMF solutions of **8** and **9** (Figure 9). Arrays **8** and **9** display similar CN stretching patterns in their Nujol mull spectra (Figure 9a). The spectrum of **8** consists of two absorptions at 2141 (s) and 2115 (s) cm^{-1}, while that of **9** consists of four absorptions at 2208 (vw), 2159 (w), 2140 (s), and 2117 (s) cm^{-1}. The absorption at 2141 cm^{-1} for **8** can be assigned to a bridging cyanide vibrational mode, in accord with the fact that cyanide ligands will shift to higher frequencies when in a bridging position than in terminal position, as described above for type **A** and **B** arrays.[21] Similarly, the absorptions at 2208, 2159, and 2140 cm^{-1} observed in the spectrum of **9** can

(23) The NMR spectra of $K_2[Ni(CN)_4]$ and $K_2[Pt(CN)_4]$ were taken in DMF solution in this work for comparison.
(24) Geary, W. *J. Coord. Chem. Rev.* **1971**, *7*, 81.
(25) (a) Huiyong, C.; Archer, R. D. *Macromolecules* **1995**, *28*, 1609. (b) Huiyong, C.; Archer, R. D. *Inorg. Chem.* **1994**, *33*, 5195.

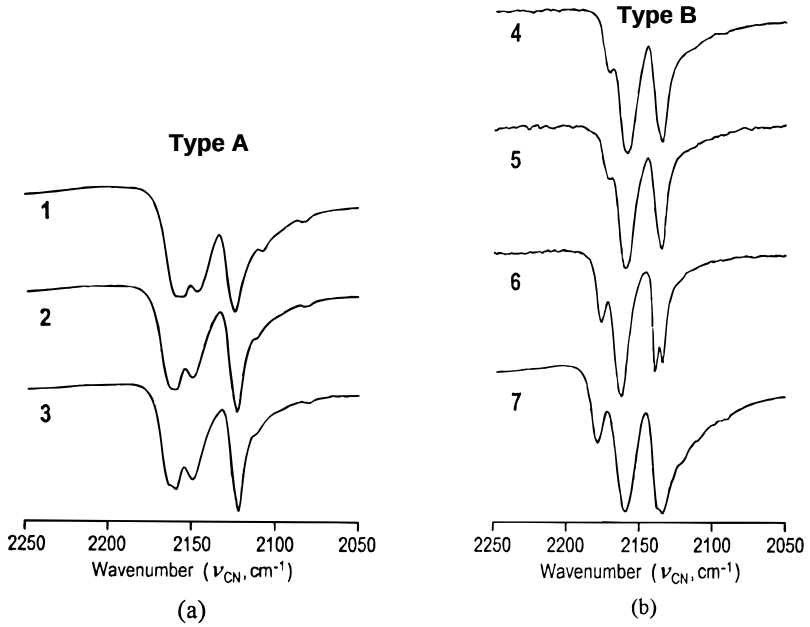

Figure 7. Solid-state infrared spectra of a) type **A** complexes **1**, **2**, and **3** and (b) type **B** complexes **4**, **5**, **6**, and **7**.

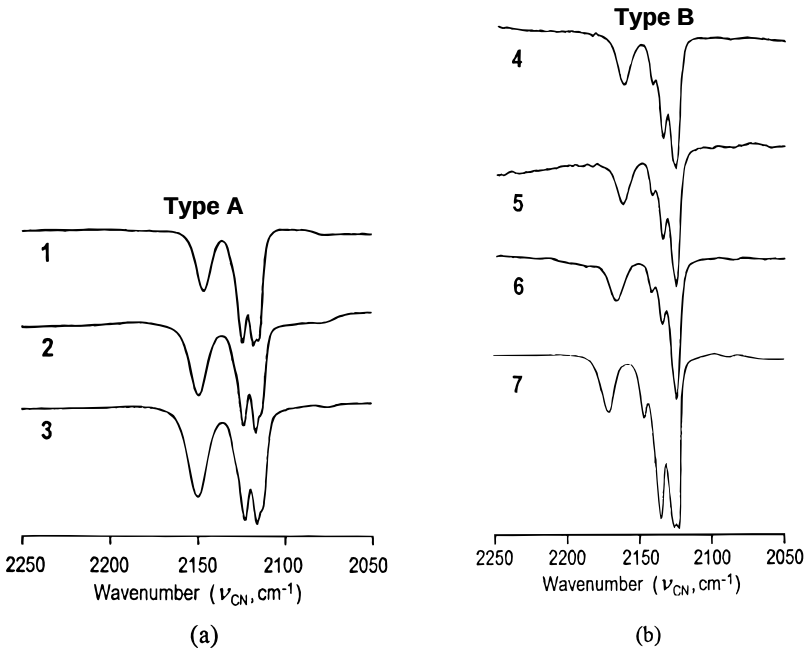

Figure 8. Solution infrared spectra of type **A** complexes **1**, **2**, and **3** and (b) type **B** complexes **4**, **5**, **6**, and **7**.

be assigned to the vibrational modes of the bridging cyanides. The remaining peaks at 2115 cm^{-1} for **8** and at 2117 cm^{-1} for **9** can be assigned to the vibrational modes of the non bridging cyanide ligands.

The solution infrared spectrum of **8** in DMF (Figure 9b) differs from its solid state spectrum. Interestingly, the spectrum is nearly identical to that of **1**, in DMF. The ^{13}C NMR spectrum of **8** in DMF displays only a resonance at 131.57 ppm due to $[Ni(CN)_4]^{2-}$ which is similar to that of **1**, in DMF. As in the type **A** and **B** complexes in solution, complex **8** is believed to be dissociated in solution and the making and breaking of Ln−N in cyanide bridges is averaged on the ^{13}C NMR time scale.

The solution spectrum of **9** (Figure 9b) in the CN stretching region also differs from its solid state infrared spectrum indicating that the solution structure is different from that of the solid. The infrared spectrum of 9 in DMA suggests that it is almost completely dissociated. The presence of $[Ni(CN)_4]^{2-}$ is indicated by a strong band at 2112 cm^{-1} while the presence of a small amount of cyanide-bridged species is indicated by a very weak band at 2146 cm^{-1}. A satisfactory ^{13}C NMR spectrum was not obtained for **9** owing to its low solubility in DMA.

Experimental Section

General Data. All manipulations were carried out on a standard high vacuum line or in a drybox under an atmosphere of dry, pure N_2. DMF (Baker) was stirred over pretreated 4 Å molecular sieves for 4−5 days in a Pyrex flask. The DMF was then degassed under vacuum, and the flask was connected to a U-tube apparatus in the drybox. The DMF was degassed a second time under vacuum and then distilled at 70−80 °C into a 1000 mL Pyrex flask at −78 °C. The DMF was then stored in the drybox. DMA (Aldrich) was stirred over BaO for 4 to 5 days in a Pyrex flask. The DMA was then degassed under vacuum and the flask was connected to a U-tube apparatus in the drybox. The

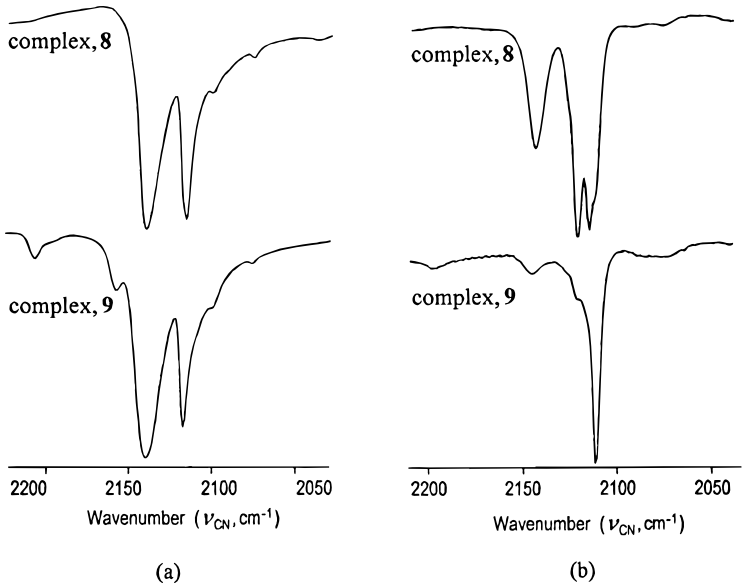

Figure 9. (a) Solid-state infrared spectra and (b) solution infrared spectra of complexes **8** and **9**.

DMA was degassed a second time under vacuum and then distilled at 70−80 °C into a 1000 mL Pyrex flask at −78 °C. The DMA was then stored in the drybox. Linde brand molecular sieves (4 Å) were heated to 150 °C under dynamic vacuum for 12−24 h prior to use.

^{13}C NMR and ^{195}Pt NMR spectra were obtained on a Bruker AM-250 NMR spectrometer operating at 62.90 and 53.77 MHz, respectively. Chemical shifts for ^{13}C NMR spectra were internally referenced to carbon-13 peaks (δ(TMS) = 0.00 ppm). Chemical shifts for ^{195}Pt were externally referenced to $\delta(K_2PtCl_6$ in $D_2O)$ = 0.00 ppm. Fourier transform infrared (FTIR) spectra were recorded on a Mattson Polaris Fourier transform spectrometer with 2 cm^{-1} resolution. Samples were prepared as solutions or Nujol mulls. Nujol samples were analyzed as films placed between KBr plates in an airtight sample holder. Solution spectra were obtained using airtight Perkin-Elmer cells with 0.1 mm Teflon spacers between KBr or NaCl windows. All IR samples were prepared in the drybox. Elemental analyses of materials were performed by Oneida Research Services, Inc. (Whitesboro, NY). Conductance measurements were obtained using a YSI model 35 conductance−resistance meter equipped with a YSI model 3401 dip cell. All measurements were performed in the drybox employing standardized solutions in DMF.

$K_2[Ni(CN)_4]\cdot H_2O$ (Strem) was dried under vacuum at 150 °C for 16 h and stored in the drybox. $K_2[Pd(CN)_4]\cdot 3H_2O$ (Aldrich) was dried under vacuum at 200 °C for 0.5 h and stored in the drybox. $K_2[Pt(CN)_4]$ (Strem) was dried under vacuum for 8 to 10 h and stored in the drybox. $ErCl_3$ (Alfa), $SmCl_3$ (Strem), $EuCl_3$ (Strem), and $YbCl_3$ (Strem) were used as received.

Preparation of the Arrays Having the General Formula $\{(DMF)_{10}Ln_2[M(CN)_4]_3\}_\infty$. The preparations of **1**−**7** are similar. In a typical synthetic procedure, a 2:3 ratio of $LnCl_3$ and $K_2[M(CN)_4]$ is allowed to react in DMF (10 mL) at room temperature over several days. (**1**: 100 mg (0.390 mmol) of $SmCl_3$ and 141 mg (0.584 mmol) of $K_2[Ni(CN)_4]$; 5 days. **2**: 76 mg (0.28 mmol) of $ErCl_3$ and 100 mg (0.415 mmol) of $K_2[Ni(CN)_4]$; up to 3 weeks. **3**: 100 mg (0.358 mmol) of $YbCl_3$ and 129 mg (0.537 mmol) of $K_2[Ni(CN)_4]$, 7 days. **4**: 102.7 mg (0.40 mmol) of $SmCl_3$ and 172.8 mg (0.60 mmol) of $K_2[Pd(CN)_4]$, 2 days. **5**: 103.3 mg (0.40 mmol) of $EuCl_3$ and 172.8 mg (0.60 mmol) of $K_2[Pd(CN)_4]$, 2 days. **6**: 111.8 mg (0.40 mmol) of $YbCl_3$ and 172.8 mg (0.60 mmol) of $K_2[Pd(CN)_4]$, 15 days. **7**: 37 mg (0.13 mmol) of $YbCl_3$ and 75 mg (0.199 mmol) of $K_2[Pt(CN)_4]$, 5 days). The resulting solution is filtered leaving a white precipitate (KCl) and a yellow (**1**−**5**) or a colorless (**6** and **7**) filtrate. The DMF is removed until a viscous oil remains. Within 24−48 h, thin platelike or chuncky X-ray-quality crystals of general formula $\{(DMF)_{10}Ln_2[M(CN)_4]_3\}_\infty$ are formed in nearly quantitative yields. **1**: Drying of the crystals under vacuum for 12−14 h results in the loss of one DMF molecule per empirical unit as determined by elemental analysis. Anal. Calcd for $C_{39}H_{63}N_{21}Ni_3O_9Sm_2$: C, 32.38; H, 4.39; N, 20.33. Found: C, 32.17; H, 4.04; N, 19.73. IR (Nujol mull of crystals, ν_{CN}, cm^{-1}): 2157 (s, sh), 2153 (s), 2144 (s), 2121 (vs) 2104 (m). IR (DMF solution, ν_{CN}, cm^{-1}): 2144 (m), 2122 (s), 2116 (s), 2113 (s, sh). $^{13}C\{^1H\}$ NMR (DMF, 303K, δ (ppm)): 131.64 (s). **2**: Drying of the crystals under vacuum for 12−14 h results in the loss of two DMF molecules per empirical unit as determined by elemental analysis. Anal. Calcd for $C_{36}H_{56}N_{20}Ni_3O_8Er_2$: C, 30.72; H, 4.01; N, 19.90. Found: C, 30.41; H, 4.27; N, 19.52. IR (Nujol mull of crystals,ν_{CN}, cm^{-1}): 2163 (s, sh), 2159 (s), 2149 (s), 2122 (vs) 2108 (m, unresolved). IR (DMF solution, ν_{CN}, cm^{-1}): 2148 (m), 2123 (s), 2116 (s) 2113 (s, unresolved). $^{13}C\{^1H\}$ NMR (DMF, 303K, δ (ppm)): 121.71 (s). **3**: Drying of the crystals under vacuum for 12−14 h results in the loss of one DMF molecule per empirical unit as determined by elemental analysis. Anal. Calcd for $C_{39}H_{63}N_{21}Ni_3O_9Yb_2$: C, 31.39; H, 4.25; N, 19.71. Found: C, 31.11; H, 3.94; N, 19.41. IR (Nujol mull of crystals, ν_{CN}, cm^{-1}): 2164 (s, sh), 2160 (s), 2150 (s), 2122 (vs) 2110 (m, unresolved). IR (DMF solution, ν_{CN}, cm^{-1}): 2150 (m−s), 2123 (vs), 2115 (vs) 2113 (s, unresolved). $^{13}C\{^1H\}$ NMR (DMF, 303K, δ (ppm)): 129.68 (s). **4**: Drying of the crystals under vacuum for 12−14 h results in the loss of one DMF molecule per empirical unit as determined by elemental analysis. Anal. Calcd for $C_{39}H_{63}N_{21}O_9Pd_3Sm_2$: C, 29.52; H, 4.00; N, 18.56. Found: C, 29.39; H, 4.11; N, 17.70. IR (Nujol mull of crystals, ν_{CN}, cm^{-1}): 2171 (m, sh), 2159 (s), 2135 (s). IR (DMF solution, ν_{CN}, cm^{-1}): 2161 (m), 2142 (m), 2134 (s), 2125 (vs). **5**: Drying of the crystals under vacuum for 12−14 h results in the loss of one DMF molecule per empirical unit as determined by elemental analysis. Anal. Calcd for $C_{39}H_{63}N_{21}O_9Pd_3Eu_2$: C, 29.46; H, 3.99; N, 18.50. Found: C, 29.47; H, 3.98; N, 17.83. IR (Nujol mull of crystals, ν_{CN}, cm^{-1}): 2171 (m, sh), 2160 (s), 2135 (s). IR (DMF solution, ν_{CN}, cm^{-1}): 2161 (m), 2142 (m), 2135 (s), 2125 (vs). **6**: Drying of the crystals under vacuum for 12−14 h results in the loss of one DMF molecule per empirical unit as determined by elemental analysis. Anal. Calcd for $C_{39}H_{63}N_{21}O_9Pd_3Yb_2$: C, 28.70; H, 3.89; N, 18.02. Found: C, 28.86; H, 3.98; N, 18.05. IR (Nujol mull of crystals, ν_{CN}, cm^{-1}): 2177 (m, sh), 2164 (s), 2139 (s), 2134 (s). IR (DMF solution, ν_{CN}, cm^{-1}): 2167 (m), 2143 (m), 2135 (s), 2125 (s). **7**: Drying of the crystals under vacuum for 12−14 h results in the loss of one DMF molecule per empirical unit as determined by elemental analysis. Anal. Calcd for $C_{39}H_{63}N_{21}O_9Pt_3Yb_2$: C, 24.63; H, 3.33; N, 15.47. Found: C, 24.99; H, 3.12; N, 15.29. IR (Nujol mull of crystals, ν_{CN}, cm^{-1}): 2179 (m), 2160 (s), 2134 (s). IR (DMF solution, ν_{CN}, cm^{-1}): 2170 (w), 2144 (w, sh), 2135 (s), 2126 (s), 2122 (s). $^{13}C\{^1H\}$ NMR (DMF, 303K, δ (ppm)): 121.20 (three-line pattern, $^1J(^{195}PtC)$ = 1016 Hz). $^{195}Pt\{^1H\}$ NMR (DMF, 303K, δ (ppm)): −4702 (s).

Preparation of $\{(DMF)_5Sm[Ni(CN)_4]Cl\}_\infty$. In a typical synthetic procedure, 107 mg (0.415 mmol) of $SmCl_3$ and 100 mg (0.415 mmol) of $K_2[Ni(CN)_4]$ are dissolved in ~20 mL of dry DMF. After 5 days of stirring at room temperature, the reaction mixture is filtered leaving a white precipitate on the frit (KCl) and a yellow filtrate. The DMF is removed until a viscous oil remains. Within 24 h, thin platelike yellow X-ray-quality crystals of $\{(DMF)_5Sm[Ni(CN)_4]Cl\}_\infty$ are formed. Drying under vacuum for 12−14 h gives the yellow solid $\{(DMF)_{0.5}Sm[Ni(CN)_4]Cl\}_\infty$ as determined by elemental analysis in nearly quantitative Yield. Anal. Calcd for $C_{17.5}H_{31.5}N_{8.5}NiO_{4.5}SmCl$: C, 31.02; H, 4.69; N, 17.57. Found: C, 31.08; H, 4.44; N, 17.28. IR (Nujol mull of crystals, ν_{CN}, cm^{-1}): 2141 (s) and 2115 (s). IR (DMF solution, ν_{CN}, cm^{-1}): 2144 (m), 2122 (s), 2116 (s), 2113 (s, unresolved). $^{13}C\{^1H\}$ NMR (DMF, 303K, δ (ppm)): 131.57 (s).

Preparation of $\{(DMA)_4Yb[Ni(CN)_4]Cl\}_\infty$. In a typical synthetic procedure, 116 mg (0.415 mmol) of $YbCl_3$ and 100 mg (0.415 mmol) of $K_2[Ni(CN)_4]$ are dissolved in ~20 mL of dry DMA. After 6 days of stirring at room temperature, the reaction mixture is filtered, leaving a white precipitate on the frit (KCl) and a light yellow filtrate. The filtrate is concentrated until small crystals are observed. X-ray-quality crystals of $\{(DMA)_4Yb[Ni(CN)_4]Cl\}_\infty$ are obtained after several days at room temperature. IR (Nujol mull of crystals, ν_{CN}, cm^{-1}): 2208 (vw), 2159 (w), 2140 (s), and 2117 (s). IR (DMA solution, ν_{CN}, cm^{-1}): 2146 (vw) and 2112 (s).

X-ray structure determination. Suitable single crystals were mounted and sealed inside glass capillaries of 0.3 or 0.5 mm diameter under N_2. Single-crystal X-ray diffraction data were collected on an Enraf-Nonius CAD4 diffractometer using graphite monochromated molybdenum Kα radiation. Unit cell parameters were obtained by a least-squares refinement of the angular settings from 25 reflections, well distributed in reciprocal space and lying in the 2θ range of 24−30°. Crystallographic data are given in Tables 1 and 3. Bond distance and angles are given in Tables 2 and 4.

The diffraction data were corrected for Lorentz and polarization effects, and absorption (empirically from ψ scan data). Only crystal for complex **1** showed significant decay and decay correction was applied (min and max corrections: 0.9752 and 0.9999). No extinction correction was necessary for all complexes. Computations were performed on a VAXstation 3100 computer using MOLEN[26] or a COMPAQ PC computer using SHELXTL.[27] Structures of **1**, **2**, **8**, and **9** were solved using the direct method MULTAN 11/82 and difference Fourier synthesis with analytical scattering factors used throughout the structure refinement.[28] Complexes **1** and **2** were found to be isomorphous with earlier reported complex **3**.[2d] Crystallographic computations for **4**−**6** were carried out using the SHELXTL program,[27] with trial structures obtained by direct method. Complexes **4**, **5**, and **6** are isomorphous with complex **7**.[2d] The direct method indicates that the space group for complexes **1**, **2**, **4**, **5**, and **6** is $P\bar{1}$, and their structures refined satisfactorily in this space group but not satisfactorily in space group $P1$. Both real and imaginary components of the anomalous dispersion were included for all non-hydrogen atoms. Structures of **4**, and **5** possess two types of rotationally disordered DMF molecules. In one rotation of the DMF ligand around the Ln−O···N axis (Figure 10a) is observed for the DMF ligand designated O3 in both complexes **4** and **5**. In the second, rotational disorder is around the Ln−O axis (Figure 10b) and is observed for DMF ligands designated O2 and O5 in complex **4** and O1 and O4 in complex **5**. The occupancies for these disordered carbon and nitrogen atoms were assigned as 0.5 while N3 atom was assigned an occupancy of 1.0. Disordered carbon atoms and nitrogen atoms were refined isotropically and the N3 atom was refined anisotropically in both **4** and **5**. Rotationally disordered DMA ligands similar to that shown in Figure 10b are observed in complex **9** and are designated O2, O3, and O4. Two positions for C and N atoms were located and refined isotropically. The occupancies for these disordered carbon and nitrogen atoms were assigned as 0.5. All remaining atoms were refined anisotropically. After all of the non-hydrogen atoms were located and refined, hydrogen atoms on the ordered DMF ligands were placed at calculated positions assuming ideal geometries with C−H distances of 0.95 Å. The thermal parameters of the hydrogen atoms were set to $B(H) = 1.3B(C)$ Å^2. Then with the positional and thermal parameters of all of the hydrogen atoms fixed, non-hydrogen atoms were refined anisotropically. New hydrogen positions were calculated, and this procedure was repeated until the parameters of the non-hydrogen atoms were refined to convergence (final shift/error ≤ 0.03 for MOLEN program[26] and 0.00 for SHELXTL program[27]).

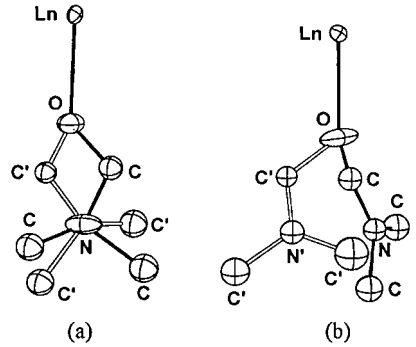

Figure 10. Rotationally disordered DMF ligands (a) around the Ln−O···N axis and (b) around the Ln−O axis.

Acknowledgment. This work was supported by the National Science Foundation through Grants CHE94-0123 and CHE97-00394.

Supporting Information Available: Listings of crystallographic data, positional parameters, anisotropic thermal parameters, bond distances, bond angles for all complexes and molecular structures of **1**, **4**, and **5** are available (53 pages). Ordering information is given on any current masthead page. Similar Supporting Information for $\{(DMF)_{10}Yb_2[Ni(CN)_4]_3\}_\infty$ and $\{(DMF)_{10}Yb_2[Pt(CN)_4]_3\}_\infty$ is given elsewhere.[2d]

IC980449H

(26) *MOLEN*, An interactive Structure Solution Procedure (developed by Enraf-Nonius, Delft, The Netherlands 1990) was used to process X-ray data, to apply corrections, and to solve and refine structures.

(27) *SHELXTL* (version 5) was used to solve and refine crystal structures from diffraction data (Siemens Energy & Automation, Inc., Madison, WI, 1994).

(28) Atomic scattering factors from *International Tables for X-ray Crystallography*; The Kynoch Press: Birmingham, UK, 1974; Vol IV.